Analytical Evaluation of the Quadruple Static Potential Integrals on Rectangular Domains to Solve 3-D Electromagnetic Problems

S. López-Peña and J. R. Mosig, *Fellow, IEEE*

Laboratoire d'Électromagnétisme et Acoustique (LEMA), École Polytechnique Fédérale de Lausanne (EPFL), EPFL-STI-ITOP-LEMA, CH-1015 Lausanne, Switzerland

In this communication, original analytical expressions for the quadruple static potential singular integrals on rectangular domains are presented. These integrals can appear when the method of moments is used to solve the mixed potential integral equation but also the electric and the magnetic static integral equations. The analytical expressions have been obtained for both source and test cells integrals when using 3-D rectangular meshes. The reported expressions can be used to solve an extensive range of electrostatic, magnetostatic and full-wave problems.

Index Terms—**Analytical integration, Green functions, integral equations (IE), method of moments (MoM), 3-D rectangular meshes.**

I. Introduction

SURFACE MIXED POTENTIAL INTEGRAL EQUATION (MPIE) formulations together with the MoM are widely used to solve electromagnetic full-wave problems. Advantageously, this formulation only implies the integration of weak singular Green functions (GFs) to fill in the method-of-moments (MoM) matrix. The singularity of these GFs is of the static type $1/R$ with $R = |\mathbf{r}-\mathbf{r}'|$ with $\mathbf{r} = (x, y, z)$ the field point and $\mathbf{r}' = (x', y', z')$ the source point. In fact, this is the same singularity found in free space static potential integral equations (IEs), both electric and magnetic. To obtain an accurate computation of this $1/R$ contribution to the MoM matrix, the GFs are usually split in a static part G_{stat} and a dynamic part G_{dyn}. The static part includes a singular term which is always proportional to the free space static potential GF $1/R$. Therefore, when low order subsectional basis functions are used, the singularity contributions to the MoM matrix can always be cast as

$$I = \iint_S \iint_{S'} \frac{1}{R} dS' dS. \tag{1}$$

In (1), S' and S are, respectively, the surfaces of the source and field patches. Several researchers ([1]–[4] among others) have broached this integral and even analytical solutions are available for triangular patches [3]. Rectangular patches can be obviously considered as combination of two triangles but it is much more advantageous to consider direct expressions which, to our knowledge are not available in the literature. This kind of patches is suitable in many electromagnetic problems. In this paper, original analytical solutions of (1) on rectangular domains will be presented as well as practical examples in which the formulas have been successfully used.

Manuscript received October 07, 2008. Current version published February 19, 2009. Corresponding author: S. López-Peña (e-mail: sergio.lopezpena@epfl.ch).

Color versions of one or more of the figures in this paper are available online at http://ieeexplore.ieee.org.

Digital Object Identifier 10.1109/TMAG.2009.2012613

II. Formulated Quadruple Integrals

We are interested here in specific versions of (1) where source and test rectangular domains (patches) are located in: a) the same plane b) parallel planes and c) perpendicular planes. In all considered cases the patches' edges are either parallel or perpendicular two by two. This produces, respectively, the following three quadruple integrals, which will be fully solved analytically

$$I_c = \int_{u_{\min}}^{u_{\max}} \int_{v_{\min}}^{v_{\max}} \int_{u'_{\min}}^{u'_{\max}} \int_{v'_{\min}}^{v'_{\max}} \frac{1}{\sqrt{(u-u')^2+(v-v')^2}} dv' du' dv du \tag{2}$$

$$I_p = \int_{u_{\min}}^{u_{\max}} \int_{v_{\min}}^{v_{\max}} \int_{u'_{\min}}^{u'_{\max}} \int_{v'_{\min}}^{v'_{\max}} \times \frac{1}{\sqrt{(u-u')^2+(v-v')^2+d^2}} dv' du' dv du \tag{3}$$

$$I_o = \int_{w_{\min}}^{w_{\max}} \int_{v_{\min}}^{v_{\max}} \int_{u'_{\min}}^{u'_{\max}} \int_{v'_{\min}}^{v'_{\max}} \times \frac{1}{\sqrt{(u-u')^2+(d_v-v')^2+(w-d'_w)^2}} dv' du' dv dw. \tag{4}$$

In these expressions, $[\mathbf{u}, \mathbf{v}, \mathbf{w}]$ represents a general system of cartesian coordinates. In (3) d is the vertical distance between cells, while in (4), d_v and d'_w respectively determine the planes in which field and source cells are placed. These quadruple integrals have all been fully solved analytically.

It is worth to set some parameters before giving the close expression of (2)–(3). So let us set $u_{11} = |u_{\min} - u'_{\min}|$, $u_{12} = |u_{\max} - u'_{\min}|$, $u_{21} = |u'_{\max} - u_{\min}|$, $u_{22} = |u'_{\max} - u'_{\max}|$, $v_{11} = |v_{\min} - v'_{\min}|$, $v_{12} = |v_{\max} - v'_{\min}|$, $v_{21} = |v'_{\max} - u_{\min}|$, $v_{22} = |v'_{\max} - v'_{\max}|$, $v_1 = u_{\min} - d'_w$, $v_2 = u_{\max} - d'_w$, $d_1 = d_v - v'_{\min}$ and $d_2 = d_v - v'_{\max}$.

The analytical form of (2) is obtained from (5). This is done by using (6) in this formula and then by simply replacing (7) in the resulting expression

$$\begin{aligned} I_c = &[I_{C2}(v_{21}, v_{22}, u_{21}, u_{22}) + I_{C2}(u_{21}, u_{22}, v_{21}, v_{22})] \\ &- [I_{C2}(v_{11}, v_{12}, u_{21}, u_{22}) + I_{C2}(u_{21}, u_{22}, v_{11}, v_{12})] \\ &+ [I_{C2}(v_{11}, v_{12}, u_{11}, u_{12}) + I_{C2}(u_{11}, u_{12}, v_{11}, v_{12})] \\ &- [I_{C2}(v_{21}, v_{22}, u_{11}, u_{12}) + I_{C2}(u_{11}, u_{12}, v_{21}, v_{22})] \quad (5) \end{aligned}$$

$$\begin{aligned} I_{C2}(x_1, x_2, x_3, x_4) = &P_c(x_1, x_3) + P_c(x_2, x_4) \\ &- P_c(x_1, x_4) - P_c(x_2, x_3) \quad (6) \end{aligned}$$

$$\begin{aligned} P_c(z, t) = &\frac{1}{2}\left[z^2 t \cdot \operatorname{arcsinh}\left(\frac{t}{z}\right)\right. \\ &\left. + \frac{\operatorname{sign}(z)}{3}(t^2 - 2z^2)\sqrt{z^2 + t^2}\right]. \quad (7) \end{aligned}$$

Similarly, the analytical expression of (3) is calculated from (8), where I_{P2} is of the form (9). The expression of P_P in this formula is shown in (10)

$$\begin{aligned} I_p = &I_{P2}(v_{21}, v_{22}, u_{21}, u_{22}) \\ &- I_{P2}(v_{11}, v_{12}, u_{21}, u_{22}) \\ &+ I_{P2}(v_{11}, v_{12}, u_{11}, u_{12}) \\ &- I_{P2}(v_{21}, v_{22}, u_{11}, u_{12}) \quad (8) \end{aligned}$$

$$\begin{aligned} I_{P2}(x_1, x_2, x_3, x_4) = &P_P(x_1, x_2) + P_P(x_3, x_4) \\ &- P_P(x_1, x_4) - P_P(x_3, x_2) \quad (9) \end{aligned}$$

$$\begin{aligned} P_p(z, t) = &\frac{z(t^2 + d^2)\operatorname{arcsinh}\left(\frac{z}{\sqrt{t^2 + d^2}}\right)}{2} \\ &+ \frac{t(z^2 + d^2)\operatorname{arctanh}\left(\frac{t}{\sqrt{t^2 + z^2 + d^2}}\right)}{2} \\ &- dzt \cdot \arctan\left(\frac{zt}{\sqrt{t^2 + z^2 + d^2}}\right) \\ &- zd^2 \cdot \operatorname{arctanh}\left(\frac{z}{\sqrt{t^2 + z^2 + d^2}}\right) \\ &- td^2 \cdot \operatorname{arctanh}\left(\frac{t}{\sqrt{t^2 + z^2 + d^2}}\right) \\ &+ \frac{(2d^2 - u^2 - v^2)\sqrt{t^2 + z^2 + d^2}}{6}. \quad (10) \end{aligned}$$

Finally, for the most involved case, the analytical solution of (4) is given by the following series of chained recursive formulas (11) to (15):

$$\begin{aligned} I_o = &I_{O2}(u_{21}, u_{22}, v_1, v_2, d_2) \\ &- I_{O2}(u_{21}, u_{22}, v_1, v_2, d_1) \\ &+ I_{O2}(u_{11}, u_{12}, v_1, v_2, d_1) \\ &- I_{O2}(u_{11}, u_{12}, v_1, v_2, d_2) \quad (11) \end{aligned}$$

$$\begin{aligned} I_{O2}(x_1, x_2, x_3, x_4, A) = &P_o(x_1, x_3, A) + P_o(x_2, x_4, A) \\ &- P_o(x_1, x_4, A) - P_o(x_2, x_3, A) \quad (12) \end{aligned}$$

$$\begin{aligned} P_o(z, t, A) &= P_{\mathrm{ash}}(z, t, A) + P_{\mathrm{atn}}(z, t, A) + P_{\mathrm{ath}}(z, t, A) \quad (13) \end{aligned}$$

$$\begin{aligned} P_{\mathrm{ash}}(z, t, A) = &Azt \cdot \operatorname{arcsinh}\left(\frac{z}{\sqrt{z^2 + A^2}}\right) \\ &+ dz^2 Azt \cdot \operatorname{arctanh}\left(\frac{t}{\sqrt{z^2 + t^2 + A^2}}\right) \\ &- d^2 z \cdot \arctan\left(\frac{zt}{A\sqrt{z^2 + t^2 + A^2}}\right) \\ &- \frac{A}{2}\left[t\sqrt{z^2 + t^2 + A^2}\right. \\ &\left. + (z^2 + A^2)\ln(t + \sqrt{z^2 + t^2 + A^2})\right] \quad (14) \end{aligned}$$

$$\begin{aligned} P_{\mathrm{ath}}(z, t, A) = &\frac{(t^3 + 3z^2 t)}{6} \cdot \operatorname{arctanh}\left(\frac{A}{\sqrt{z^2 + t^2 + A^2}}\right) \\ &+ \frac{A(3z^2 - A^2)}{12} \cdot \operatorname{arctanh}\left(\frac{t}{\sqrt{z^2 + t^2 + A^2}}\right) \\ &- \frac{z^3}{3} \cdot \arctan\left(\frac{At}{z\sqrt{z^2 + t^2 + A^2}}\right) \\ &+ \frac{At}{3}\sqrt{z^2 + t^2 + A^2} \\ &+ \frac{A(z^2 + A^2)}{4}\ln(t + \sqrt{z^2 + t^2 + A^2}) \quad (15) \end{aligned}$$

$$\begin{aligned} P_{\mathrm{atn}}(z, t, A) = &\frac{z(z^2 + 2t^2 + d^2)}{4} \cdot \arctan\left(\frac{zA}{t\sqrt{z^2 + t^2 + A^2}}\right) \\ &- \frac{z(z^2 - A^2)}{12} \cdot \arctan\left(\frac{zA(z^2 + 2t^2 + A^2)}{t(z^2 - A^2)\sqrt{z^2 + t^2 + A^2}}\right) \\ &+ z^2 A \cdot \ln\left(\left|2t\sqrt{z^2 + t^2 + A^2} + (z^2 + 2t^2 + A^2)\right|\right) \\ &- \frac{z \cdot \ln\left(\left|2t\sqrt{z^2 + t^2 + A^2}\right| - (z^2 + 2t^2 + A^2)\right)}{4} \\ &+ \frac{t^3}{3}\operatorname{arctanh}\left(\frac{\mathrm{A}}{\sqrt{z^2 + t^2 + A^2}}\right) \\ &- \frac{A(3z^2 + A^2)}{6}\operatorname{arctanh}\left(\frac{\mathrm{t}}{\sqrt{z^2 + t^2 + A^2}}\right) \\ &+ \frac{z^3}{3}\arctan\left(\frac{tA}{z\sqrt{z^2 + t^2 + A^2}}\right) \\ &+ \frac{At\sqrt{z^2 + t^2 + A^2}}{6}. \quad (16) \end{aligned}$$

It has to be remarked that when doing these calculations an enormous casuistry depending on x_1, x_2, x_3, x_4, and A appears in (12). This casuistry is not reported in this communication because of its size, nonetheless it has to be studied to properly apply the formula.

III. Results

The reported formulas can be used to solve an extensive set of numerical electromagnetic problems. Here, three applications related to IE-MoM formulations are shown. Firstly, the induced charge in the walls of a perfect electric conducting (PEC) cuboid

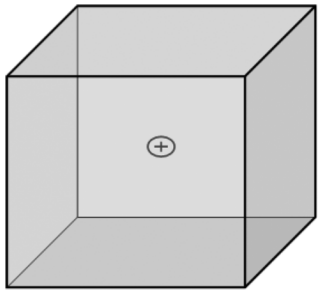

Fig. 1. Enclosed unitary electric charge by a PEC cuboid of 100 mm size. Equation (17) is set on the cavity walls to obtain the induced charge on the metallic shield by using the MoM. The cavity has been uniformly meshed with 600 square cells of the same size. Sub-domain pulse basis functions have been defined over these cells.

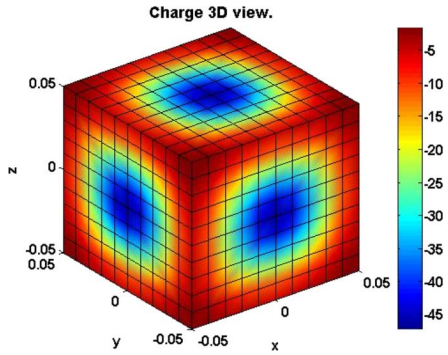

Fig. 2. Resulting ρ_s on the cavity walls when solving the problem in Fig. 1 with MoM. The total value of charge on the shield is of -1.003 C, that means a relative error is of 0.3% The problem has been solved reaching a speed of 14 758 integrals/s (processor Intel Pentium IV at 3.2 GHz, 1 GB of RAM).

housing a centered electric positive unitary charge, as shown in Fig. 1, is obtained. This has been done by solving the following electrostatic integral equation with the MoM

$$\frac{1}{|\mathbf{r}-\mathbf{r_q}|}+\int_{S'}\frac{\rho_s(\mathbf{r}')}{|\mathbf{r}-\mathbf{r}'|}dS'=0\Bigg|_{\forall \mathbf{r}\in S}. \tag{17}$$

The first term of (17) is the potential produced by the shielded point charge placed at $\mathbf{r_q}$ on the cavity walls S', while the second term is the potential produced by the unknown cavity wall surface charge distribution ρ_s on itself. The cavity has been uniformly meshed with 600 square cells, over which sub-domain pulse basis functions are defined. The resulting induced surface density charge on the cavity walls is shown in Fig. 2. Here, it can be observed that the result is fully coherent with theory since the charge distribution is symmetrically distributed, is concentrated in the center of the enclosure walls and has negative sign. An excellent check of the numerical accuracy achieved is the fact that the resulting total value of charge on the shield is of -1.003 C, so that the relative error is of 0.3% which it is a very good result in terms of precision. The problem shown in figure has been solved reaching a speed of 14 758 integrals/s (processor Intel Pentium IV at 3.2 GHz, 1 GB of RAM). Hence, it can be stated that the reported formulation is also competitive in terms of efficiency.

Next, our formulas (5)–(16) are used to calculate numerically the static GF G of a PEC empty rectangular cavity. This GF

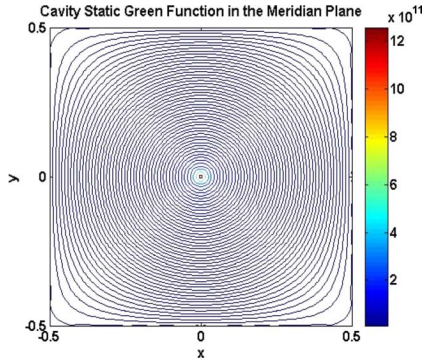

Fig. 3. Cut in the meridian plane containing q of the numerical approach of G for $\mathbf{r}'=\mathbf{r}_c$. The isolines have symmetry of revolution rounding the point $\mathbf{r}'=\mathbf{r}_c$ and match the boundary condition on the cavity walls. The singular phenomenon at $\mathbf{r}'=\mathbf{r}_c$ is fulfilled. The physical GF behavior is well recovered.

is solution of the following differential equation with Dirichlet boundary conditions ($G=0$) on the cavity walls:

$$\nabla^2 G(\mathbf{r},\mathbf{r}')=\delta(\mathbf{r}-\mathbf{r}'). \tag{18}$$

The left-hand side of (18) is the laplacian of the GF, while the right hand side represents mathematically an electric positive unitary charge q, which is enclosed by the cavity. Fig. 1. represents the problem when the position $\mathbf{r}'$ of q is the center of the enclosure. Within this context, G has the physical meaning of the electrostatic potential inside the cavity and can be written as

$$G(\mathbf{r},\mathbf{r_q})=\frac{1}{|\mathbf{r}-\mathbf{r_q}|}+\int_{S'}\frac{\rho_s(\mathbf{r}')}{|\mathbf{r}-\mathbf{r}'|}dS'. \tag{19}$$

In this formula, two contributions can be distinguished, which come respectively from q (the free space term) and from the induced charge ρ_s on the walls. A discrete version of the induced charge can be calculated for any position $\mathbf{r_q}$ of q by solving (17) with the MoM, as it has been shown in the previous problem. If ρ_s in (19) is replaced by the samples of this discrete version, then a numerical approximation for G is obtained. The needed integrals to solve (19) are also computed analytically, since they are intermediate steps to find (5)–(16). In Fig. 3, the obtained numerical results for G are shown in a cut in the meridian plane containing q. The values have been calculated by replacing the discrete version of ρ_s shown in Fig. 2, in (19). In Fig. 3, it is appreciated that the isolines of G have symmetry of revolution rounding the point $\mathbf{r}'=\mathbf{r_q}$ and match the boundary condition on the cavity walls. Besides also in this figure, it is observed that the singular phenomenon at $\mathbf{r}'=\mathbf{r_q}$ is fulfilled. These facts allow stating that the physical GF behavior is well recovered.

Finally, (5)–(16) are applied to the resolution of a full-wave problem. This problem consists of calculating the S parameters of the combline-like resonator [5] shown in Fig. 4. Here, it can be appreciated that the resonator is loaded with the typical structures appearing in a combline filter (mushrooms, tuning posts, ground-connected cables). The problem has been solved with an MPIE-MoM strategy by expanding the electric equivalent currents on the metallic surface of the enclosed structures by means of rooftop basis functions. Rooftops are defined over rectangular cells and approximated by a pulse of the same volume.

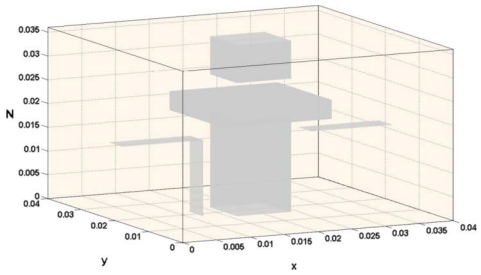

Fig. 4. Resonator loaded with the typical structures appearing in a combline filter (mushrooms, tuning posts, ground-connected cables). An MPIE-MoM strategy is used to calculate the S parameters of this resonator. The shielded structures are meshed with rectangular cells. Rooftop basis functions are defined over these cells. A δ-gap tension generator has been used to model an electric excitation field.

A δ-gap tension generator has been used to model an electric excitation field. The GFs related to the problem are split in a static part $G_{\rm stat}$ and a dynamic part $G_{\rm dyn}$. The expressions of these GFs can be found in [6]. It is worth here to recall the following generic formulations of the static part:

$$G_V = \frac{1}{4\pi\varepsilon}\sum_{m=-M}^{M}\sum_{n=-N}^{N}\sum_{l=-L}^{L}\sum_{i=0}^{7} \times \frac{V_i}{\sqrt{(X_i+2ma)+(Y_i+2nb)+(Z_i+2lc)}} \quad (20)$$

$$G_A^{ss} = \frac{\mu}{4\pi}\sum_{m=-M}^{M}\sum_{n=-N}^{N}\sum_{l=-L}^{L}\sum_{i=0}^{7} \times \frac{A_i^{ss}}{\sqrt{(X_i+2ma)+(Y_i+2nb)+(Z_i+2lc)}}. \quad (21)$$

Expression (20) is related to the scalar potential V, while (21) is associated to the vector potential $\mathbf{A}$. Both expressions have been found by using image theory, so that they are obtained from the free space static potential GF $1/R$. In (20) and (21), $s \in \{x, y, z\}$, $V_i = \pm 1$, $A_i^{ss} = \pm 1$, $X_i = x \pm x'$, $Y_i = y \pm y'$, $X_i = z \pm z'$, and (a, b, c) are the cavity dimensions along (x, y, z). The contribution of these GFs to the MoM matrix when using a Galerkin procedure can be analytically calculated with (5)–(16). In Fig. 5, the S parameters linked to the structure in Fig. 4 are shown. This result has been produced with an experimental code developed in the frame of an ESA-ESTEC contract called COFRESITO which uses the formulation reported here. With our approach only the metallic surfaces need to be discretized. We have compared in Fig. 5 our approach with results obtained with the commercial software HFSS (finite elements and hence 3-D volume discretization). For meshes of comparable linear size, our unrefined approach produced, with a few hundred unknowns, results sensibly similar to those of HFSS using tens of thousand unknowns. Indeed for this highly sensitive resonant structure the frequency deviation between the two approaches was only about 1.38%.

IV. Conclusion

In this paper, original analytical expressions to calculate the quadruple integral of the $1/R$ potential singularity have been reported. These formulas are useful when using rectangular cells and low order basis functions within an IE-MoM context. The formulation reported here exhibits a high degree of flexibility, since they can be used in several 2-D or 3-D IE problems. Here, results for both static and full-wave IE situations have been shown. The MPIE has been used in the full-wave case because it has a static potential type singularity. It has been also shown that this analytical formulation is competitive in terms of efficiency and accuracy. Dense meshed problems have been solved quickly and a very good agreement has been obtained when comparing with the commercial software HFSS (based on the finite elements method). There is plenty of room for speeding-up our strategy, particularly in the image series expansion and in the treatment of $G_{\rm dyn}$. Therefore, prospects are strong for improving its accuracy while reducing the computer time. With the strong analytical preprocessing introduced in this paper, our surface-based approach should be really competitive.

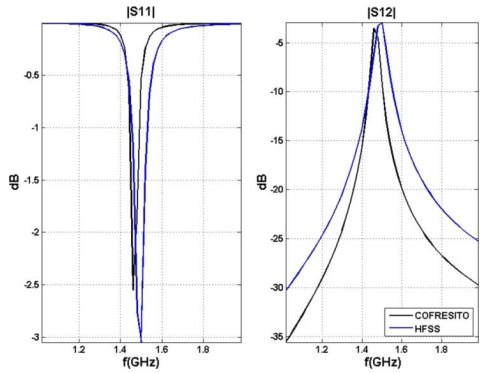

Fig. 5. S parameters linked to the structure in Fig. 4. Result produced with the experimental code COFRESITO developed in the frame of an ESAESTEC contract. This code uses the formulation reported in this paper. The S parameters agree very well with the commercial software HFSS (the frequency deviation at the resonance frequency is 1.38%).

Acknowledgment

The authors would like to thank Dr. M. Mattes for his invaluable scientific help. This paper was supported in part by ESA-ESTEC under Contract 16332/02/NL/LvH.

References

[1] D. R. Wilton, S. M. Rao, A. W. Glisson, D. H. Schaubert, O. M. Al-Bundak, and C. M. Butler, "Potential integrals for uniform and linear source distribution on polygonal and polyhedral domains," *IEEE Trans. Antennas Propag.*, vol. AP-32, no. 3, pp. 276–281, Mar. 1984.

[2] R. D. Graglia, "On the numerical integration of the linear shape functions times the 3-D Green's function or its gradient on a plane triangle," *IEEE Trans. Antennas Propag.*, vol. 41, no. 10, pp. 1448–1455, Oct. 1993.

[3] T. F. Eibert and V. Hansen, "On the calculation of potential integrals for linear source distributions on triangular domains," *IEEE Trans. Antennas Propag.*, vol. 43, no. 12, pp. 1499–1502, Dec. 1995.

[4] P. Arcioni, M. Bressan, and L. Perregrini, "On the evaluation of the double surface integrals arising in the application of the boundary integral method to 3-D problems," *IEEE Trans. Microw. Theory Techn.*, vol. 45, no. 3, pp. 436–439, Mar. 1997.

[5] F. Arndt, V. Catina, and J. Brandt, "Efficient hybrid EM CAD and optimization of a comprehensive class of advanced microwave filters," presented at the Int. Workshop Microw. Filters (CNES), Tolouse, France, Oct. 2006.

[6] S. López-Peña, M. Mattes, and J. R. Mosig, "The impact of metallic scatterers on the performance of a class of shielded structures," presented at the Eur. Conf. Antennas Propag. (EuCAP), Edinburgh, U.K., November 2007.